EUROPEAN COMMISSION
5th EURATOM FRAMEWORK PROGRAMME 1998-2002
KEY ACTION : NUCLEAR FISSION

HTR-M

European Project for the development of HTR Technology - Materials for the HTR

CONTRACT N°
FIKI-CT-2000-00032
FIKI-CT-2001-00135

CHEMICAL KINETIC DATA FOR ADVANCED OXIDATION MODELS

by

K. Kuhn, H-K Hinssen, R. Moormann

FZJ

Dissemination level : CO
Document Number: HTR-M-02/12-D-3.3.56
Deliverable 3.4

Chemical kinetic data for advanced oxidation models

1 Introduction

Due to their excellent mechanical and thermal properties carbon-based materials are used in High Temperature (HTR) Reactors for basic components: Fuel elements and reflectors of HTRs are made from graphite. Because of their limited oxidation resistance at high temperatures accidents, leading to contact of oxidizing gases (air or steam) with these carbon components, have to be considered in safety analyses: Oxidation may induce fission product release, may weaken the strength of components and may destroy protecting structures by explosion of flammable mixtures, formed during these events. Severe air ingress with graphite burning is probably the only credible event, which may lead to a pronounced release of the radioactive inventory of modern small HTRs; however, excluding sabotage, war, airplane crash beyond the scope usually taken into account in safety analyses etc., the frequencies of severe air ingress are nearly negligibly small (which means by order of magnitudes smaller than those of core meltdown events of LWRs. On the other hand, the extended safety concept of modern small HTRs requires answers on the safety behaviour until deep into the 'hypothetical' (very low frequency) range. In steam cycle HTRs steam/water ingress accidents belong to design basis accidents and accordingly, the graphite oxidation degree has to be worked out for these accidents; because of the endothermic character of the steam/water reaction, a burning like process as in air ingress cannot occur.

To some extent, carbon oxidation takes place in the normal operating reactor too, due to impurities of the cooling gas (particularly steam). In general, selection of carbon materials has to take into account their oxidation resistance as an important criterion. Alltogether, *graphite oxidation is to a large extent a safety-relevant problem* but also *a general material one*. Safety analyses on air and steam interaction with carbons require detailed knowledge of the respective oxidation kinetics.

Considerable experimental and theoretical work has been performed in 1965-85 on graphite oxidation in HTRs in EU-countries (mainly F, UK, D) and in USA, Japan and Russia. Analytical tools for examination of graphite oxidation in air and steam ingress accidents and in normal operation have been developed; kinetic experiments on relevant graphites in steam and oxygen have been done and also experiments simulating flow/oxidation under conditions near to the real air ingress accident ones. Nevertheless, some important lack of knowledge

remained. Besides that, most work was concentrated on the needs of large and medium sized HTRs and is not completely applicable to modern small HTRs without separate decay heat removal system; some graphite oxidation problems specific for these small HTRs have not yet been solved.

This report consists of:

- Generation of oxidation kinetics data, which are input values for advanced graphite oxidation models (oxygen/air and steam): These models allow a better understanding of the time behaviour of severe air ingress accidents in HTRs, but in addition give information on the depth of penetration of the oxidation process into the porous carbon. The latter is relevant in order to estimate the time, which remains until first coated particles are attacked by oxygen and (in case of steam ingress events) allow for calculation of UO_2-oxidation respectively carbide fuel hydrolysis of defective particles. In this report, the generation of chemical kinetics data is described for selected carbon materials, relevant for HTRs. It should be noted however, that advanced oxidation models require besides the chemical reactivity depending on burn-off also the effective diffusion permeability of the oxidizing gas within the carbon; respective measurements remain to be done for most of these materials. This report contains also a typical application of an advanced oxidation model using the code PROFIL and kinetic data generated.

2 Experiments

Most of the experimental investigations were done in the THERA and the INDEX facilities. Experiments take place in the chemical reaction controlled regime I and in the in pore diffusion controlled regime II. For explanation of these regimes see for example [7] and page 8 respective chapter 3.1 of this report. The thermogravimetric apparatus THERA was used for the regime I. In regime II higher flow rates are necessary, which can be generated in the INDEX apparatus. Long-term experiments at low temperatures in air (673 and 773 K) were done in an annealing furnace.

2.1 The THERA facility

The THERA facility is an simultaneous thermal analyser where the experimental unit is coupled with the weighing system. So the weight loss of the investigated material can be measured directly during oxidation. The gas supply system in this facility is disposed for reaction gas (which can be mixed with an additional gas via an second inlet) and inert gas. The exhaust unit can be coupled with a mass spectrometer or, in case of steam experiments, with an external weighing system to control the amount of H_2O which was injected during runtime.

The samples used in the THERA facility are small pieces of maximum 250 mg. The temperature, partial pressure and flow rate of reaction and inert gas is held constant during the experiments. The temperature of the samples is controlled over a thermocouple inside of the sample holder, which is situated beneath the sample. Measurements of the weight loss occur with an computerised program and can be observed over the whole runtime with an stipulated measuring interval of 20 s. A schematic presentation of the THERA facility is given in Fig. 2-1.

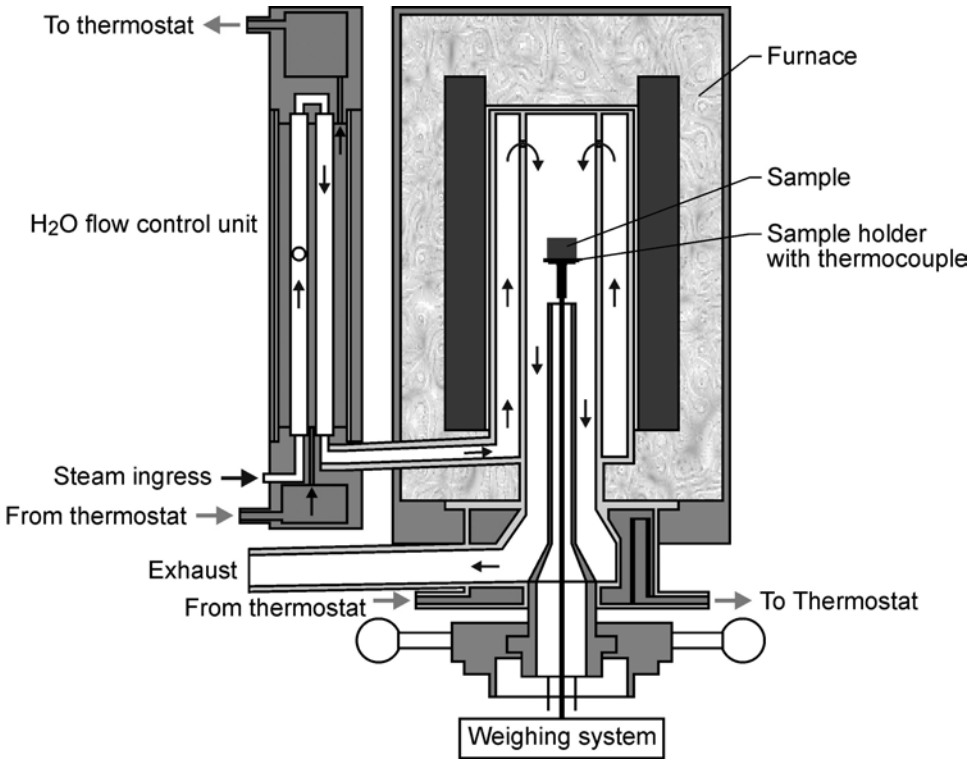

Fig. 2.1: Scheme of the experimental unit of the THERA facility

2.2 The INDEX facility

The INDEX facility is an inductive heated oxidation experiment, with a gas supply system for reaction gas, inert gas and product gas. In the sample cavity, a tube shaped graphite sample can be heated very fast over an inductive heating unit whereas the reaction gas flow through the sample. Thereby a oxidation reaction between the reaction gas and the inner borehole of the sample take place. During the experiment the outer region of the sample is rinsed with inert gas. Overpressure of the inert gas according to the reaction gas prevent the contact of the reaction gas with the outer surface of the sample. The reaction, inert and product gas, emitting at the exhaust can be measured by mass spectrometry.

The samples used in this facility have an outer diameter of 20 mm, an inner diameter of 10 mm and a total length of 30 mm. During the experiments temperature, composition and partial pressure of the reaction gas are constant. After a temperature- and reaction gas rate dependent duration of max 4 h, the supply of the reaction gas stopped and the sample cooled down and get weighed. The total weight loss is determined from the amount of the weight differences

over the whole experiment in relation to the oxidation surface. A schematic presentation of the INDEX facility is given in Fig. 2-2.

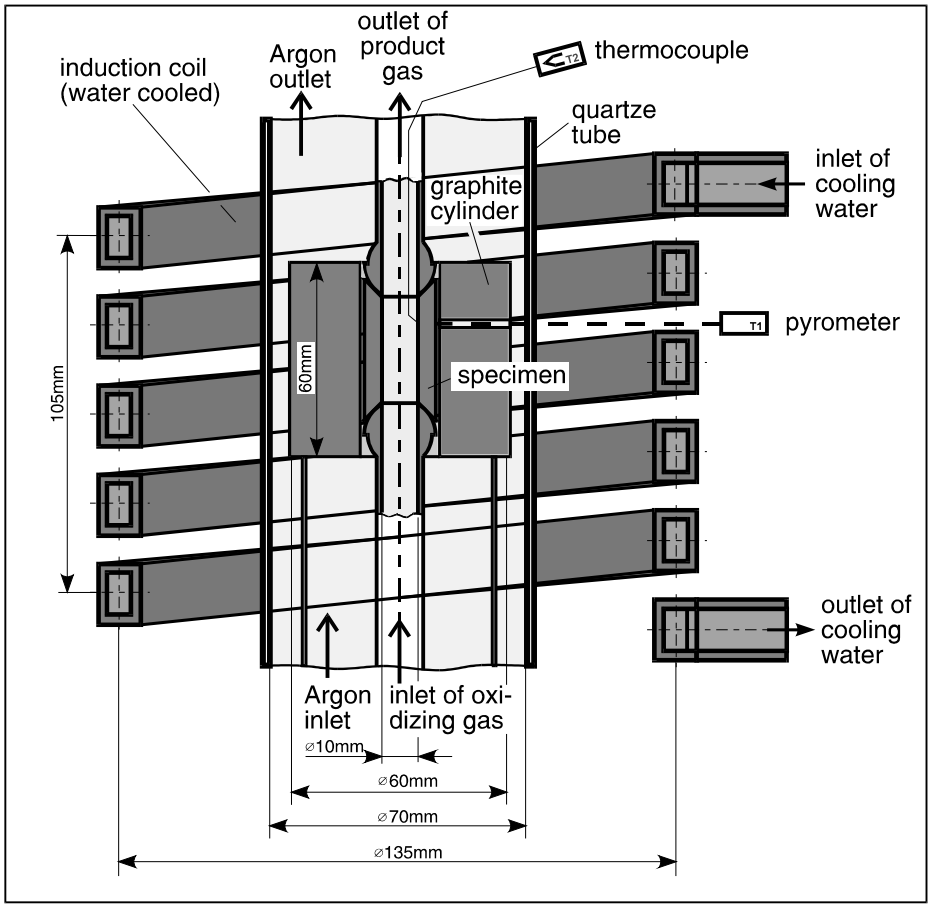

Fig. 2-2: Scheme of the central part of the oxidation facility INDEX

2.3 Investigated Materials

The different investigated C-based materials are HTR nuclear graphites, whereas one of the material containing an amount of 30 % of Si. The doping of Si into the carbon implicates a higher density and a lower porosity and is agreed to increase the oxidation resistance of the material by formation of an impermeable SiO_2-layer. The HTR graphites can contain different filler and binder materials or the filler and binder graphite consists from the same pitch coke. The main data of the investigated materials, which are discussed in this report, are given in Tab. 2-1. Not listed in this table are Ti-doped carbons, where oxidation measurements revealed an insufficient behaviour (no protection by TiO_2); these materials are no longer in consideration for nuclear application (fusion, HTR).

Tab.: 2-1: Investigated materials

Material	Description	Density [kg/m^3]	Ash-content [ppm / %]	Si-content [%]
A3-3	HTR fuel element matrix graphite (90 % filler graphite / 10% coked phenolic resin binder)	1730	≤ 60	-
A3-27	HTR fuel element graphite (90% filler graphite / 10% coked synthetic resin binder)	1740	≤ 60	-
V483T	Fine grain nuclear graphite (filler: pitch coke; binder: pitch)	1810	200-340	-
ASR-1RG	Nuclear graphite (filler: pitch coke; binder: pitch)	1790	1500	-
ASR-1RS	Nuclear graphite (filler: spec. pitch coke; binder: pitch)	1820	200	-
RG	Well graphitised standard HTR graphite	~1750	<200	-
SiC 30	composite SiC-graphite	2650	<0,1%	30

2.4 Experimental conditions

The experiments in regime I were performed under isothermal conditions at temperatures between 673 – 1073 K in air, and between 1173 – 1273 K in steam. Regime II measurements in steam are done at 1273 K, older regime II measurements in oxygen [1,2,3] not listed in this table, cover a temperature range of 923 – 1123 K. The partial pressures diversified between ambient pressure (annealing furnace), 1 bar in air and 1.05 / 1.1 bar in steam (THERA / INDEX). The reason for slightly overpressure in experiments in steam in the THERA and INDEX facilities is to inhibit air ingress in the cavity from the exhaust. The final weight losses diversified between ~ 60 and 100 % and the run times between 8 – 1300 h in air and between 18 – 61 h in steam. The experimental conditions are given in Tab. 2-2.

Tab. 2-2: Experimental conditions

T [K]	Material	Reaction gas	Facility	P	Gas flow rate
673*	A3-3 A3-27 ASR-1RG ASR-1RS V483T	Air	Annealing furnace	1 atm	natural gas convection
773	A3-27 V483T SiC 30	Air	Annealing furnace	1 atm	natural gas convection
923	A3-27	Air	THERA	1 bar	200 [ml/min]
1023	A3-27	Air	THERA	1 bar	200 [ml/min]
1173	A3-3 V483T RG	Steam	THERA	1.05 bar	6-8 [l/h]
1253	A3-3 V483T RG	Steam	THERA	1.05 bar	6-8 [l/h]
1273	V483T A3-27	Steam	INDEX	1.1 bar	310 [l/h]

*= published in [4]

2.5 Results

Experiments in air

The experimental investigations in air show as expected a strong temperature dependence of the reaction rate. At low temperature (773 K) long-term experiments with a run time of 800 – 1300 h are necessary to reach burn off values above 50 %. In case of V483T and SiC 30 these values however could not be reached within a reasonable time span. Here a burn off of 30 % (V483T) and 10 % (SiC 30) can be observed after 1300 h run time (Fig. 2-3).

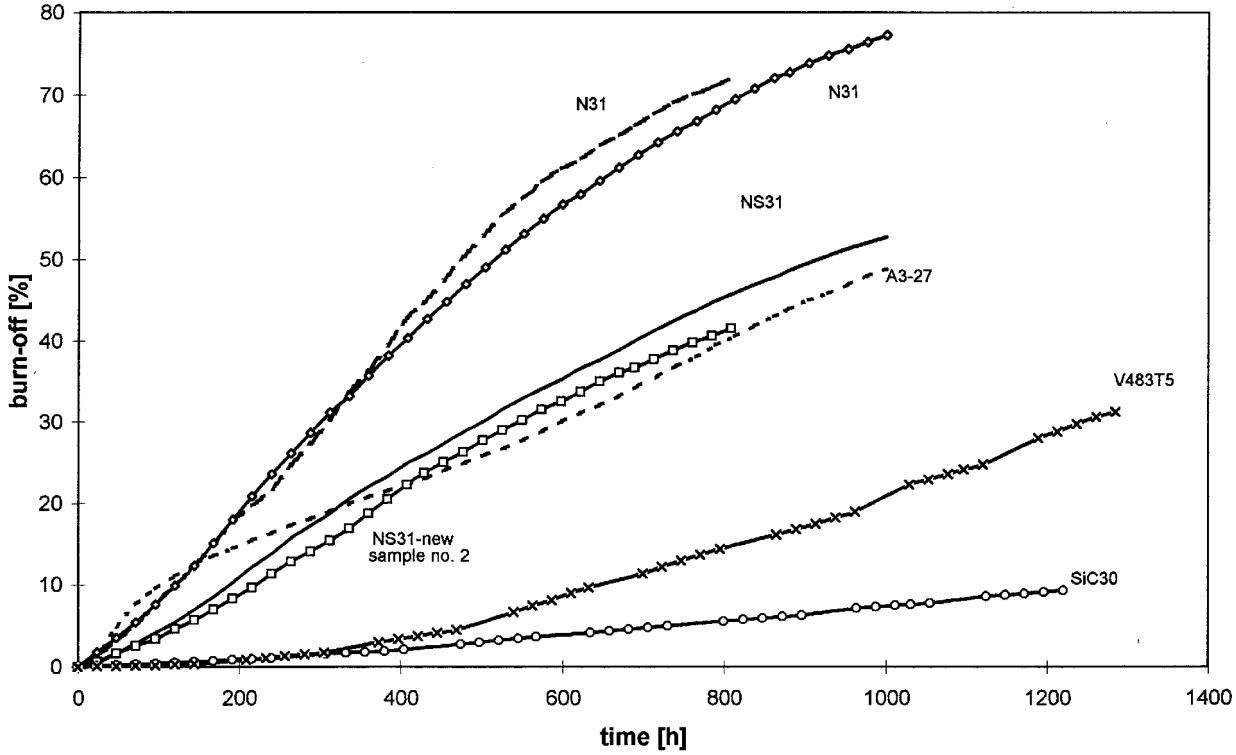

Fig. 2-3: Burn off versus time for different C-based materials in air at 773 K.

The nuclear graphites show rate increases with burn off (up to 40 % burn off) followed by a nearly linear decrease in regime I. An example for this behaviour is given in Fig. 2-4 for the HTR graphite V483T5. This material show a burn off by a factor of 4 between virgin material and rate maximum, the calculated activation energy for this purpose is 166 kJ/mol.

The formation of rate maxima can be explained by the kinetics of carbon oxidation. At low temperatures (regime I) the chemical reaction itself is the rate limiting step, the material oxidised homogeneously within the pore system (see chapter 3). A strong burn off dependence of rate is due to the changing of the reactive surface during the oxidation process: Posity increases by enlarging of the inner surface at low burn off, whereas at high burn off the pore walls vanish by oxidation and the reactive surface diminish. So the reactivity (inner surface) reaches a maximum at medium burn off values [5].

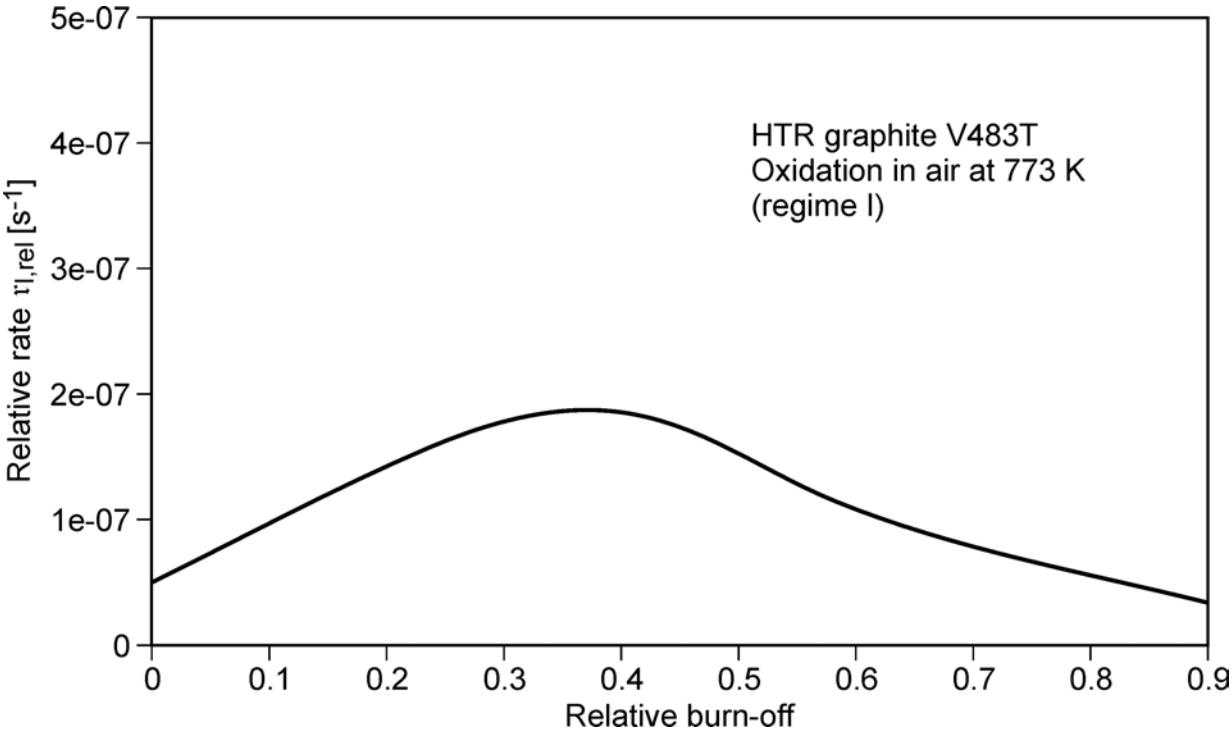

Fig. 2-4: V483T: burn off vs. rate (relative) at 773 K.

In case of the fuel element matrix graphite A3-27 two peaks can be observed at 5 and 35 % burn off in regime I. The rate versus burn off profiles for temperatures between 673 – 1023 K in regime I are given in Fig. 2-5. The observed two rate maxima can be explained by a selective binder-filler oxidation. The first peak at 5% burn off is most probably due to the oxidation of the binder, at 35% burn off the second peak shows the oxidation of the filler graphite. At higher temperatures the second peak becomes more pronounced and the binder peak vanishes. The activation energies, which are different for binder and filler, are given in Fig. 2-5. The lower activation energy of the binder is responsible for the vanishing of the binder peak at higher temperatures. Experiments in regime II revealed apparent activation energies substantially larger than one halve of the values of regime I [6], which is not completely consistent with the standard theory of reaction kinetics in porous carbons.

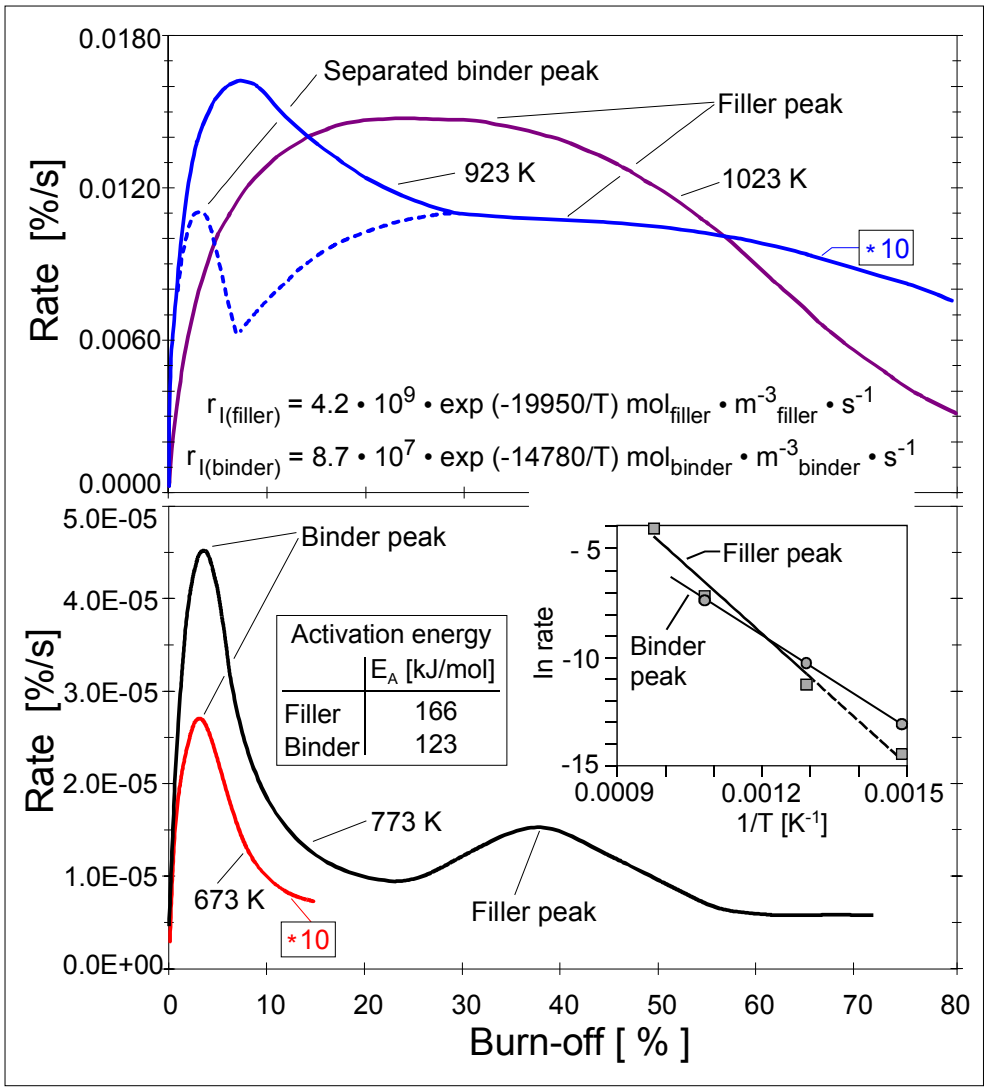

Fig. 2-5: Air oxidation of A3-27 matrix graphite in regime I

Experiments in steam

After steam oxidation in the chemical reaction controlled regime I (1173 and 1253 K) in the THERA facility an limited volume loss with a simultaneous higher porosity can be observed in all samples (Fig. 2-6). Thereby the decrease of the size of each sample is relatively low, which is in line with the expectations for regime I.

All samples were analysed after oxidation at 1173 K with ICP-MS.

[Here measurements are done from samples after oxidation in steam at 1173 K, to present ash analyses in relation to impurities of the materials. The results of these analyses are not yet available.]

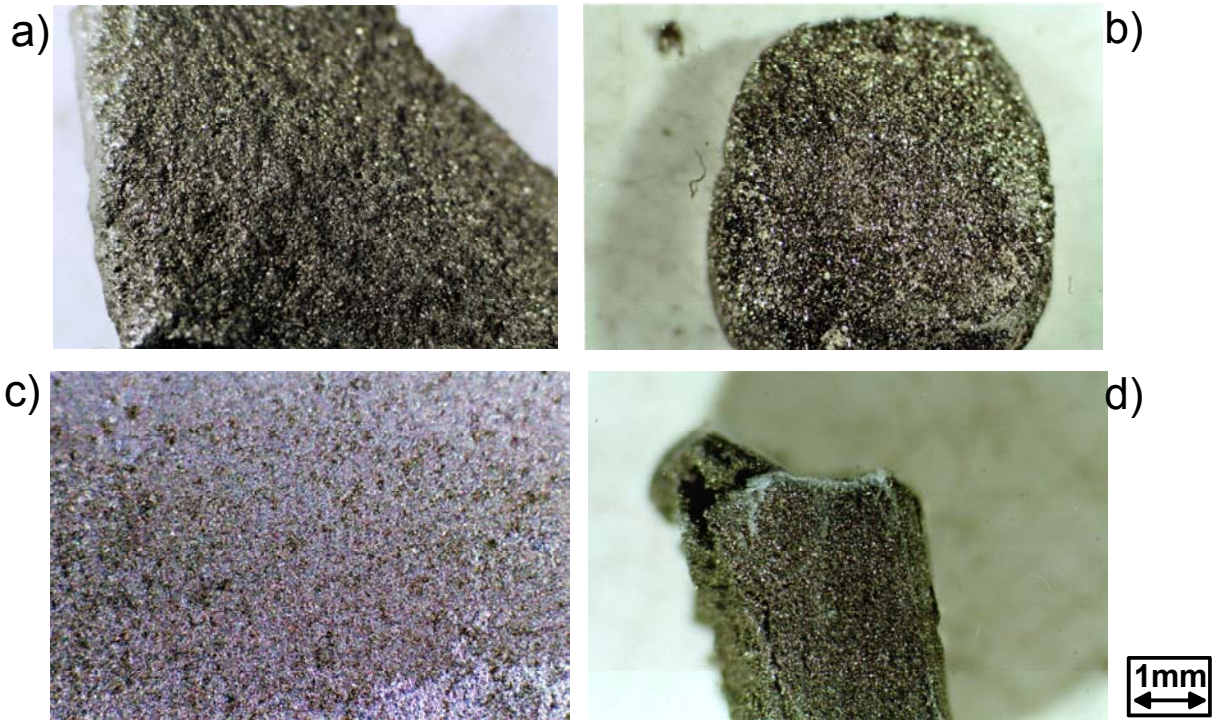

Fig. 2-6: Examples of investigated C-based materials. Left: unoxidised material; Right: samples after oxidation in steam. a), b) = A3-3; c), d) = V483T.

The presentation of the results from experiments in the chemical reaction controlled regime are given in Fig. 2-7 – 2-10. Fig. 2-7 and 2-8 contain the burn off versus time curves for the materials and Fig. 2-9 and 2-10 the reaction rates versus burn off, which are evaluated from the burn off over time values.

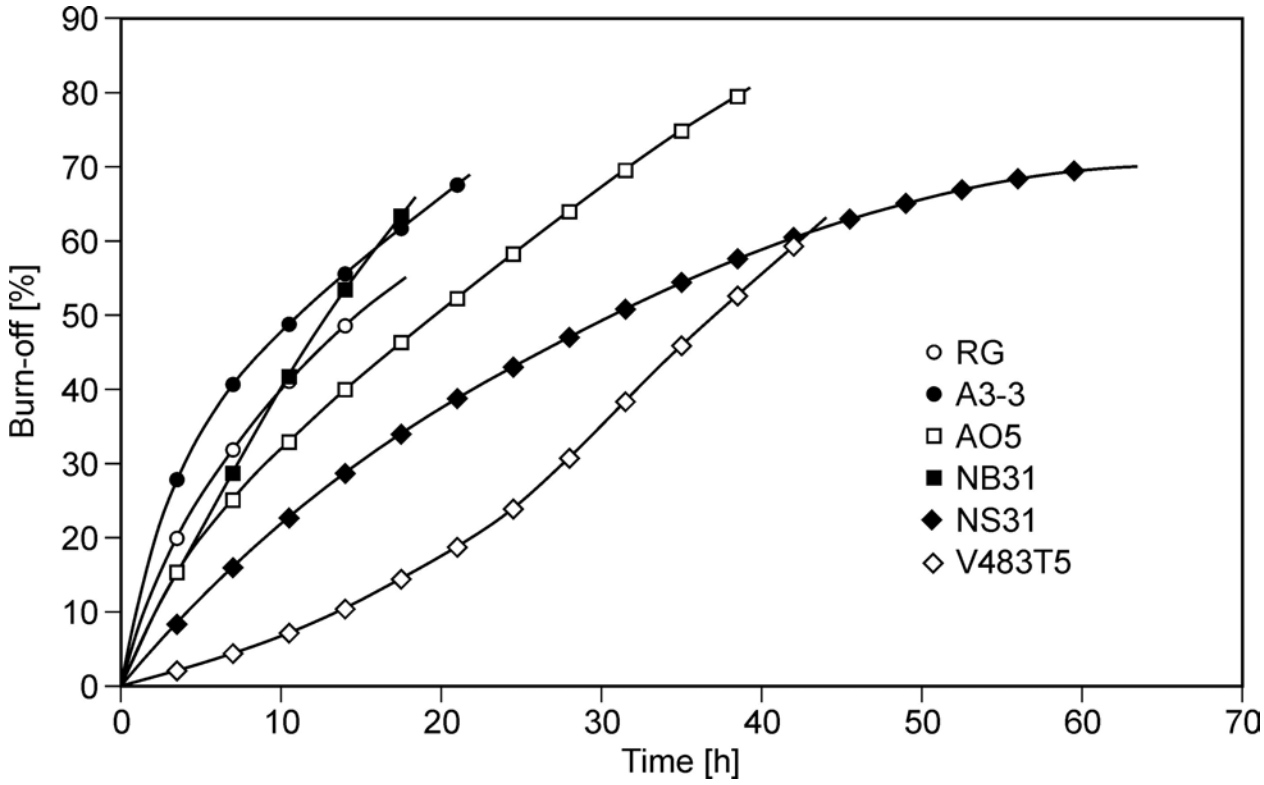

Fig. 2-7: Burn off vs. time for Oxidation in steam at 1173 K

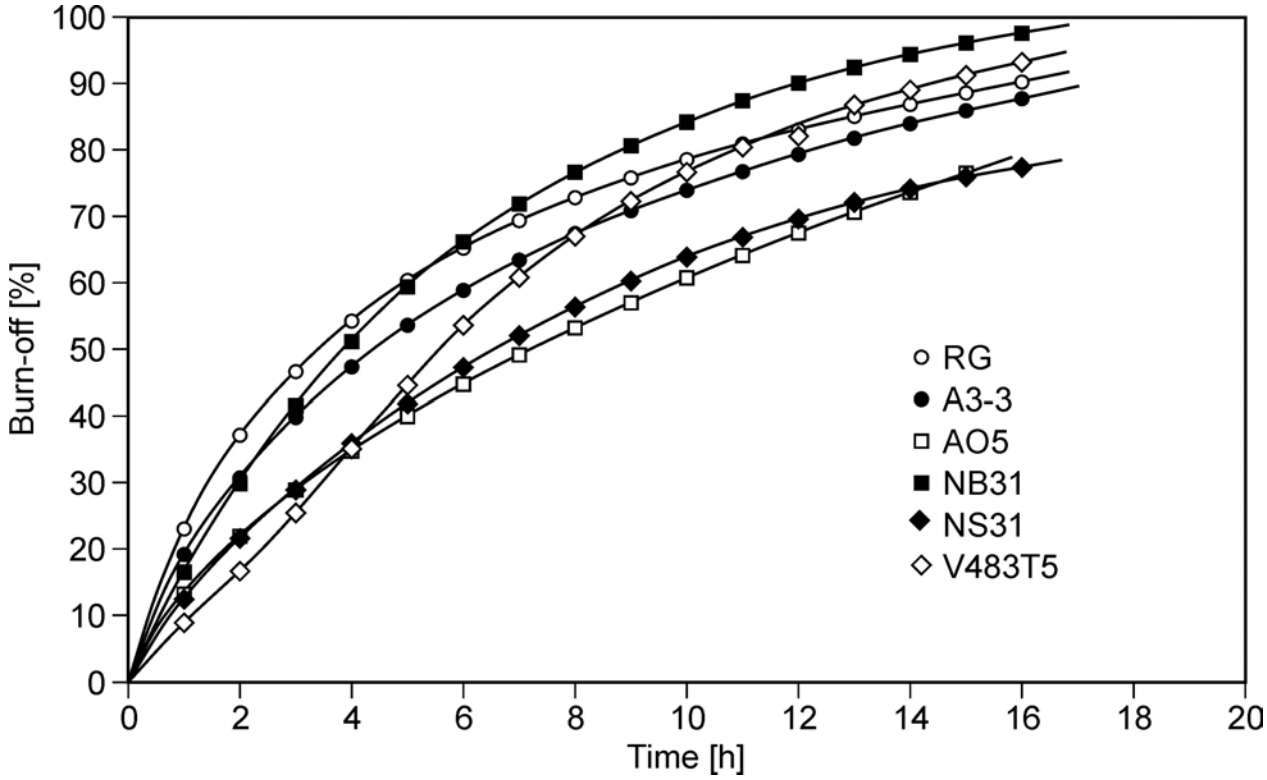

Fig. 2-8: Burn off vs. time for Oxidation in steam at 1253 K

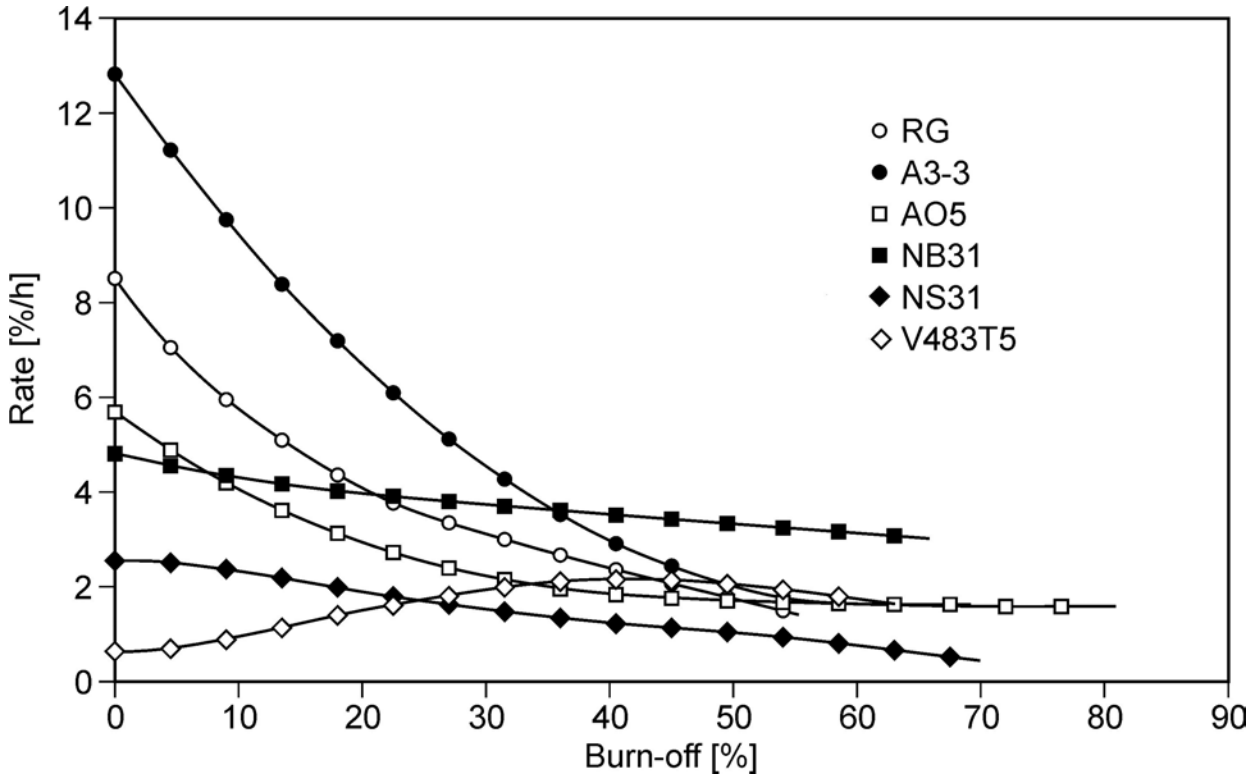

Fig. 2-9: Rate vs. burn off for oxidation in steam at 1173 K

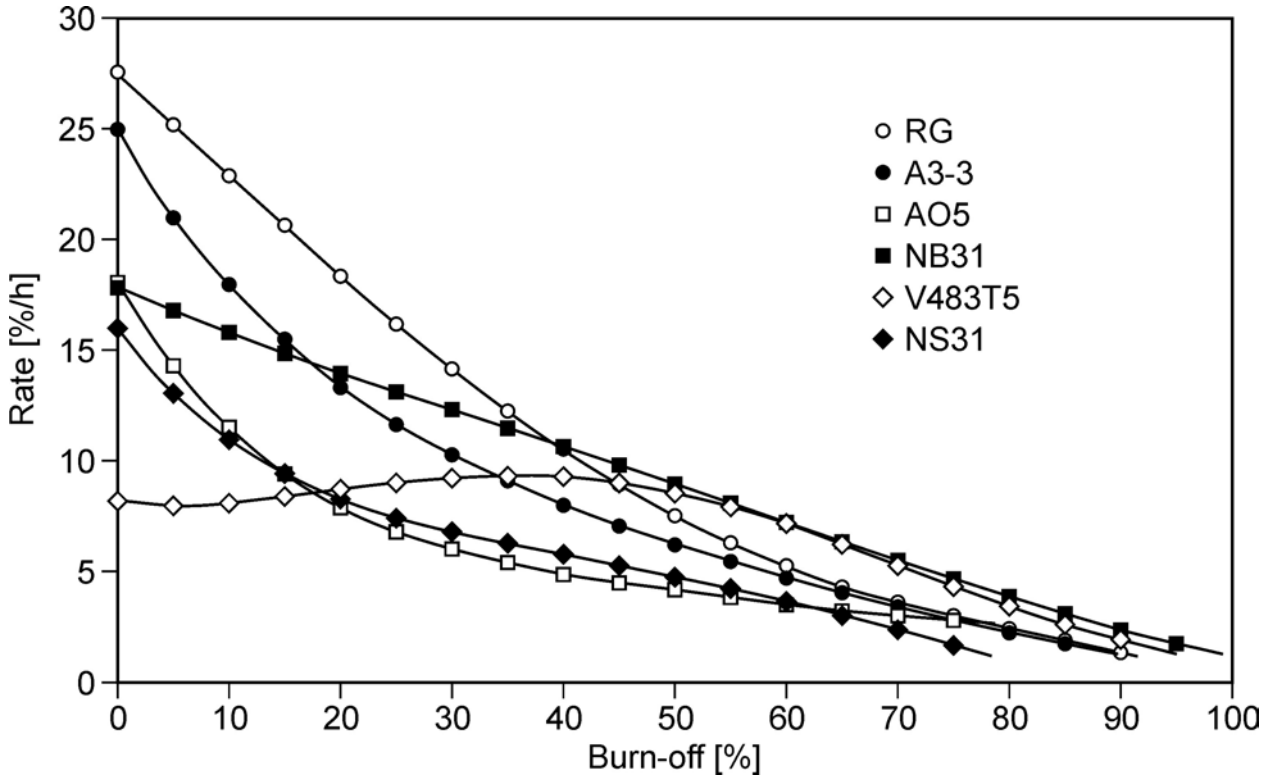

Fig. 2-10: Rate vs. burn off for oxidation in steam at 1253 K

It becomes obvious from these figures, that (except of V483T at 1173 K) with increasing burn off the oxidation passing slower and at 1253 K the reaction is about 2 (A3-3) up to 6 times faster (V483T) in relation to 1173 K (Fig. 2-7 and 2-8). The samples show roughly the same oxidation versus burn off behaviour at both temperatures. So with increasing burn off the reaction rates decrease (Fig. 2-9 and 2-10). Only for the nuclear graphite V483T a rate maximum was found at both temperatures. The HTR graphites A3-3 and RG show the highest reaction rates at both temperatures up to 20 respective 40 % burn off.

On the basis of reaction rates at two temperatures the activation energies were calculated for 10 and 40% burn off. With increasing burn off the activation energies decrease. This tendency is to be observed at all investigated materials in regime I. The average activation energies are given in Tab. 2-3.

Tab. 2-3: Average activation energies

Material:	**E_A [kJ/mol]**
A3-3	117 +/- 18
V483T	271 +/- 50 ($325_{(10)} - 216_{(40)}$)
RG	216 +/- 5

The results from experiments in the in pore diffusion controlled regime are given in Fig. 2-11. The shape of rate versus burn off curves in regime I is different from that in regime II where usually a plateau is formed. The explanation for this behaviour is give in detail in chapter 3. It should be noted, that the regime I/II transition does not only depend in temperature, but also on sample size (see chapter 2.1 and 2.2): INDEX samples have to be for experimental reasons of remarkably larger size than those of THERA; larger size decrease the transition temperature. Oxidation in regime II is usually accompanied by some erosion mass loss, which is due to the high flow rates in combination with the oxidation induced strength loss.

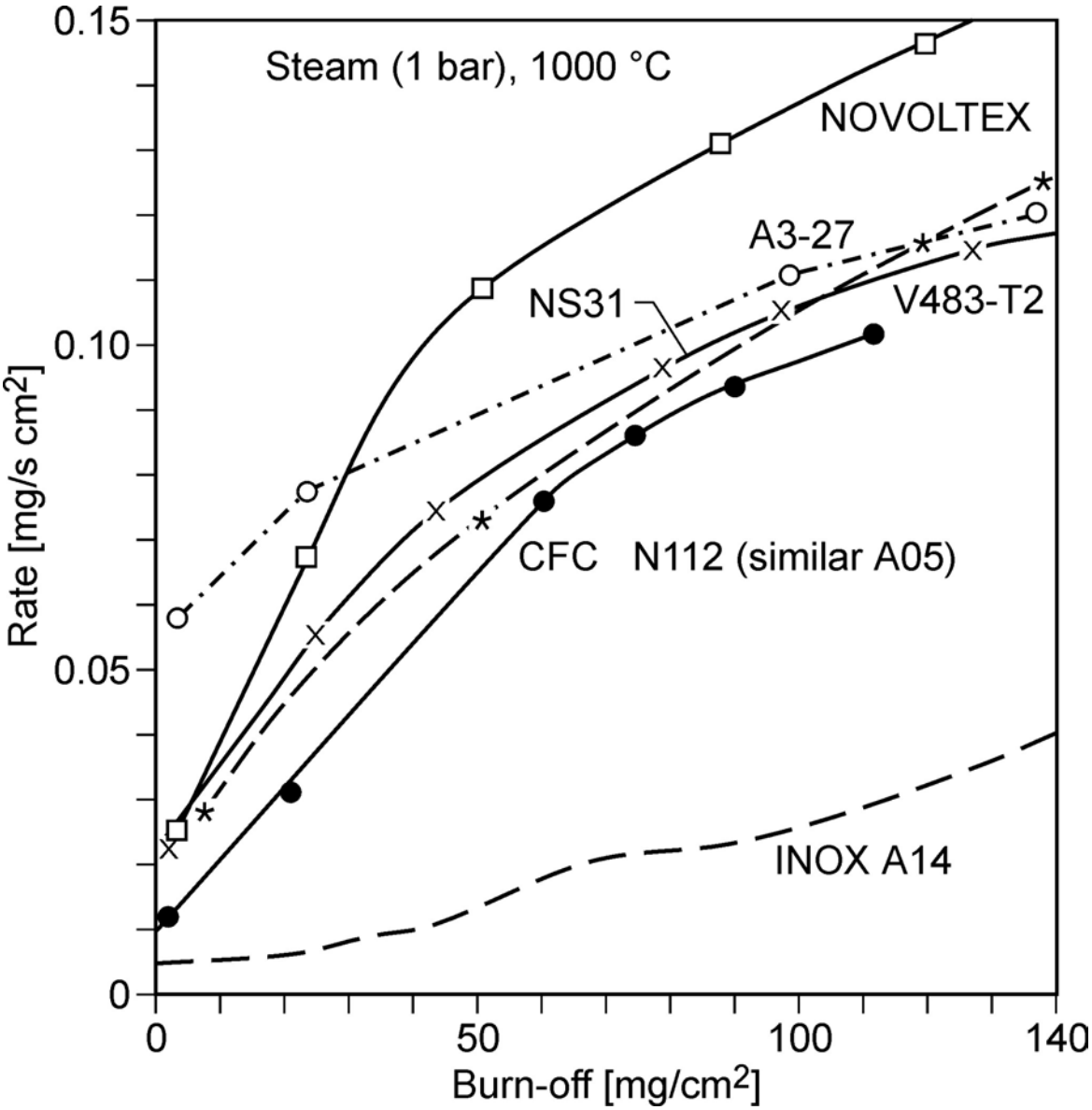

Fig. 2-11: Burn off versus rate for different C-Based materials in steam at 1273 K

3 Kinetic data

3.1. Carbon oxidation

There are several overviews on carbon oxidation [6,7,8] available.

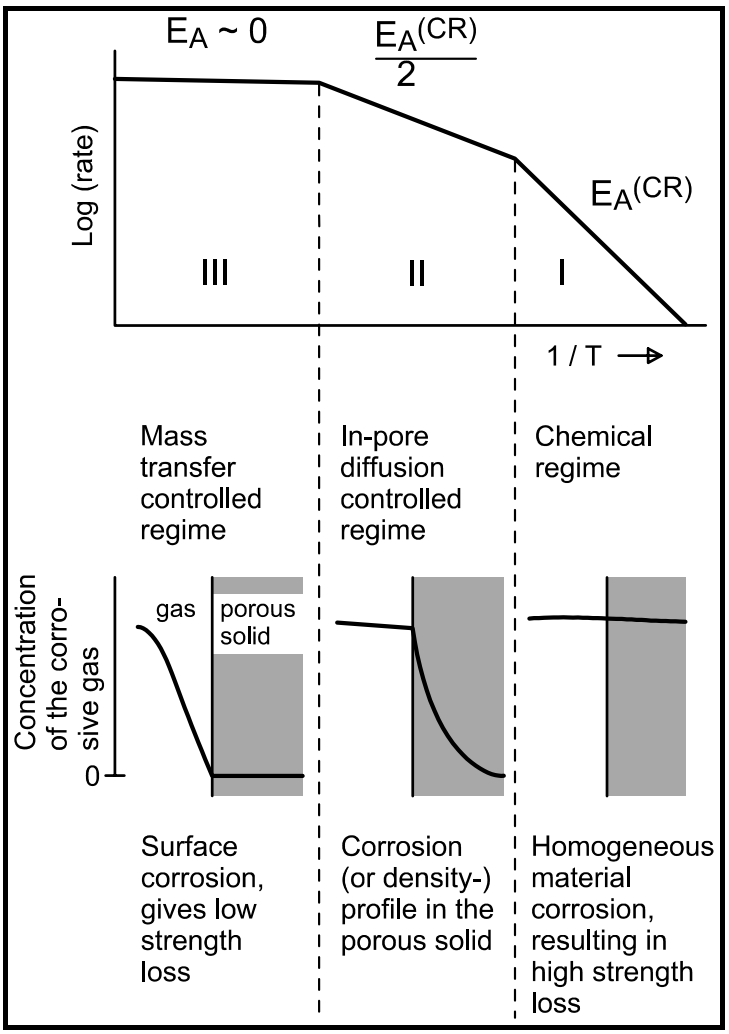

Fig. 3-1: Schematics of oxidation regimes

With respect to reactions between gases and homogeneous porous solids with gaseous products 3 reaction zones have to be distinguished: Fig. 3-1 shows schematically these regimes and their typical temperature dependences (E_A = activation energy). At low temperatures (regime I) the chemical reaction itself is the rate limiting step and the material is oxidised homogeneously within the pore system, which leads to a severe loss of mechanical strength. A strong dependence of rate r_1 on volume related burn-off B (here used as relative value normalised with the burn-off of the virgin material) with a pronounced maximum is found, because reactive surface is changed in course of the oxidation. Rates for small concentration ranges of the oxidising gas are given as:

$$r_I = k_{vO} \exp(-E_A/RT)\, c_e^{n} \cdot f_I(B) \quad [mol \cdot m^{-3} \cdot s^{-1}] \qquad (1)$$

(n = reaction order, k_{v0} = rate constant, c_e = educt gas concentration). For larger concentration ranges a Hinshelwood-Langmuir type equation has to be used, which also consideres inhibition by reaction products (see right-hand side of eqn. (2)).

At intermediate temperatures (regime II), consumption of the oxidizing gases within the pores becomes important and, accordingly, the oxidation attack becomes smaller in depth of the material; this is due to the fact, that the temperature dependence of the chemical process is much larger than that of the competing in-pore gas diffusion. Therefore, a concentration and - as a consequence of that - a burn-off (oxidation) gradient within the carbon is found. For integral, isothermal rates an increase with (surface related) integral burn-off B up to a plateau value is usually observed [6]. Assuming carbon as homogeneous with respect to gas transport and reactivity, the following equation, which is a superposition of second Ficks law and rate equation of regime I, has to be solved (written here for Hinshelwood-Langmuir kinetics) [9]:

$$\varepsilon \frac{\partial c_e}{\partial t} = D_{eff} \cdot \frac{\partial^2 c_e}{\partial x^2} - \frac{k_{v0} \cdot \exp(-E_{A1}/RT) \cdot c_e}{1 + k_1 \cdot \exp(-E_{A2}/RT) \cdot c_e + k_3 \cdot \exp(-E_{A3}/RT) \cdot c_{pr}} \qquad (2)$$

where c_{pr} is the product gas concentration, x is material depth, ε is the transport porosity, D_{eff} is the effective gas diffusivity within the graphite and k are rate constants. The solution of eqn. (2) is substantially complicated by the fact, that D_{eff} and k (particularly k_{v0}) depend significantly on the local burn-off; this burn-off dependence is rarely known in a sufficient manner. The relation to the integral rates r_{II} of regime II is given by the concentration gradient on the geometrical surface:

$$r_{II} = -\left(D_{eff} \cdot \frac{\partial c_e}{\partial x} \right)_{x=0} \qquad [mol \cdot m^{-2} \cdot s^{-1}] \qquad (3)$$

Due to the aforementioned problems in course of solution of eqn. (2) of advanced carbon oxidation models, isothermally measured rates r_{II} are mainly used; this however has the disadvantage, that nonisothermal processes cannot be exactly modelled and that information on depth of oxidation attack is not obtained. Fitting equations for r_{II} use solutions of eqn. (2) for $B=0$ containing an empirical burn-off dependence $f_{II}(B)$; as an example, the following expression for isothermal rates r_{II} is based on kinetics as in eqn. (1):

$$r_{II} = k_{II} \cdot \exp(-0.5 \cdot E_A/RT) \cdot c_e^{(n+1)/2} \cdot f_{II}(B) \quad [mol \cdot m^{-2} \cdot s^{-1}] \qquad (4)$$

with (for $B=0$): $k_{II} = \sqrt{k_{vo} \cdot D_{eff}} \cdot 2/(n+1)$ $[mol^{(1-n)/2}/(m^{0.5-1.5n} \cdot s)]$

At high temperatures (regime III) external mass transfer to the outer surface is the rate limiting step and the reaction is restricted to the geometrical surface only; mass transfer rules are applied here for rate calculations which means, that kinetics is not influenced by properties of the solid.

Table 3-1 contains approximate transition temperatures between different oxidation regimes (valid strictly for $n=1$ and $B=B=0$; $l = V/S_{exposed}$, with $S_{exposed}$ = geometrical surface of the specimen exposed to the oxidising gas, V = specimen volume; β=mass transfer coefficient). The transition I-III omitting regime II occurs for $\beta < D_{eff}/l$ resp. $Sh/x_l < R/x$ (Sh = Sherwood number and x_l = characteristic length of specimen - as defined by theory of analogy in flow and mass transfer).

Transition	Transition Temperature [K]
I-II	$-E_A \Big/ \left(R \cdot \ln\left[\frac{D_{eff}}{k_{v0} \cdot l^2} \right] \right)$
II-III	$-E_A \Big/ \left(R \cdot \ln\left[\frac{\beta^2}{k_{v0} \cdot D_{eff}} \right] \right)$
I-III	$-E_A \Big/ \left(R \cdot \ln\left[\frac{\beta}{k_{v0} \cdot l} \right] \right)$

Tab 3-1: Approximate transition temperatures between oxidation ranges

Main purposes of this part are (a) presenting representative data for burn-off dependent regime I rates of nuclear carbons and effective diffusivities and (b) discussion of numerical solutions of eqn. (2) for selected conditions.

3.2. Burn-off dependent reactivities and effective diffusivities

Reactivities

This chapter summarises the interpretation of the experimental work, done within 5th European Framework program for kinetic data on advanced oxidation models.

The carbon oxidation behaviour of different advanced materials are in detail different in air and in steam as may be seen by comparison of figures 2-4 to 2-11. Apart from the generation

of two peaks at A3-3 and A3-27 (explained in chap. 2.5) all HTR graphites built up peak maxima during oxidation in air. In steam these maxima could not be observed expect of the V483T. The exact shape of rate versus burn off curves is obviously different in both gases. There is no increase of reactivity observed during oxidation in steam (beside the V483T): here the reaction rates and activation energies decrease with increasing burn off. In the moment we are not able to explain this behaviour. Anyway the sequence of the oxidation resistance for different materials is, for example in comparison of A3-27/A3-3 to V483T, roughly the same in air and in steam, but with rate in air at 923 K comparable to those in steam at 1173 K. This behaviour can be explained by the fact, that the activation energies are higher in steam than in air because of the endothermic character of the steam/carbon reaction.

Effective diffusion permeabilities and related properties (literature survey and older measurements of our group)

Effective diffusion coefficients in porous carbons may be measured by static [10] or transient [11] methods; only transient methods are able to cover the effect of blind pores, which are affected by oxidation, too. A systematic comparison of static and transient results is still to be done. Measurement of diffusion permeabilities at different pressures allow for determination of contribution of Knudsen diffusion and gives data on the average pore radius [10]: For A3 matrix graphite it was shown by static measurements, that a substantial contribution of Knudsen diffusion may occur at least at low burn-off in gas mixtures containing light gases; further on, opening of closed micropores at low burn-off (air oxidation 673 K) led to a significant decrease of the average (transport) pore radius $\bar{r}$ of A3-27 from 0.57 μm (virgin) to 0.17 μm (burn-off 0.05); its diffusion permeability ψ ($=D_{eff}/D$) increased in this burn-off range from $1 \cdot 10^{-3}$ to $7 \cdot 10^{-3}$. Later measurements for a burn-off up to 0.25 indicated a ψ-value of 0.125 and a re-increase of $\bar{r}$ to 0.4 μm. It should be noted here, that -due to different behaviour (see 2.5) of binder and filler- these results depend on temperature. Fig. 3-2 contains permeabilities ψ and pore radius $\bar{r}$ of graphite V483T depending on burn-off for oxidation in air. Results are similar to A3-27 except of ψ -values for virgin material being 1 order of magnitude larger for V483T and of the missing re-increase of $\bar{r}$ when burn-off reaches 0.25 for V483T. For burn-off dependence of diffusion permeability holds here: $\psi \sim B^{1.7}$.

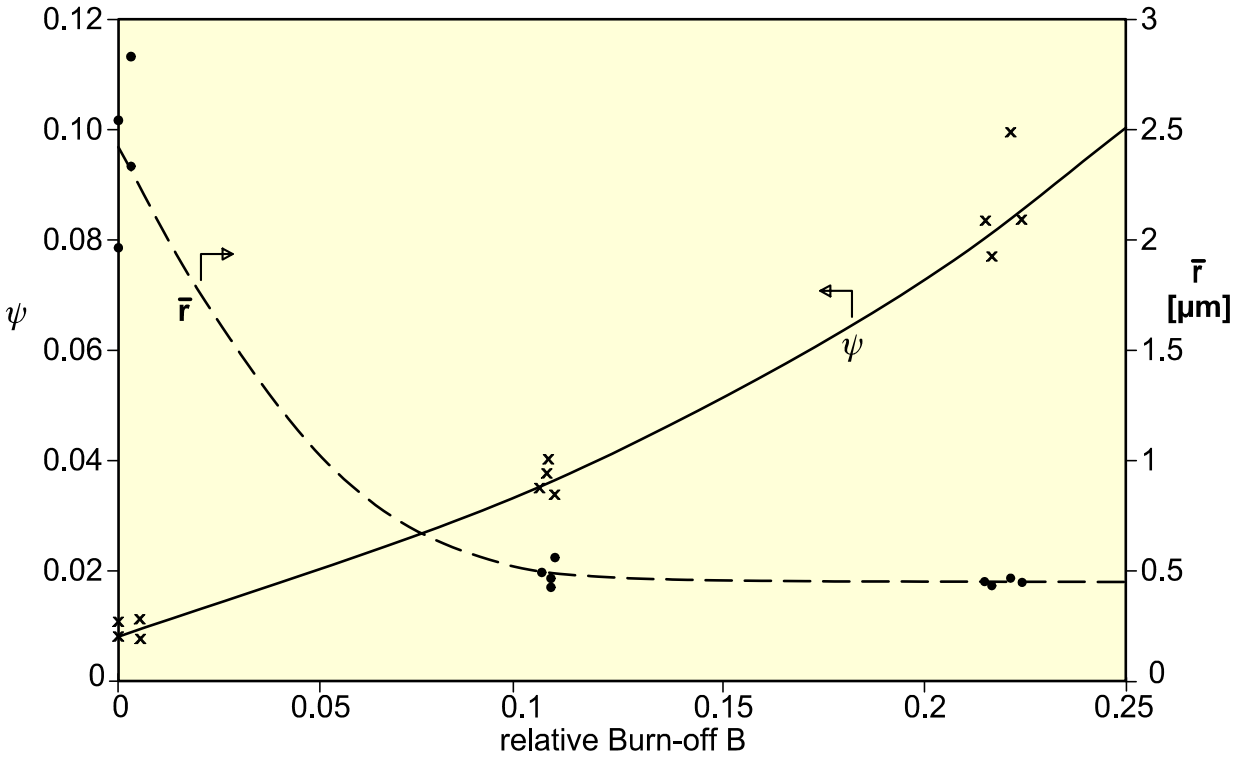

Fig. 3.2: Burn-off dependent diffusion permeability ψ and average transport pore radius $\bar{r}$ of V483T graphite (static measurements).

3.3 Numerical Solutions of Transport/reaction Equation

Numerical solutions of eqn. (2) are performed for V483T graphite because of its homogeneous character. Burn-off dependence of reactivity and permeability used are those of chapter 3.2. Oxidation medium is air at 0.1 *MPa*; a temperature independent Hinshelwood-Langmuir term $k_{01} = k_1 \cdot \exp(-E_{A1} / RT) = 0.35\ [m^3 / mol]$ is applied. No hindrance by external mass transfer (regime III) is taken into account. Geometry of a plane sheet (thickness = 0.02 *m*) is assumed with oxidation from both major surfaces.

At first, relevance of instationary calculations were proven: Based on Crank [12] it was shown, that quasistationary conditions ($dc_e/dt = 0$) are usually allowed in solution of equation (2), because time constants for reaching diffusion/reaction equilibrium under constant burn-off are small compared with characteristic times, which are required for variation of burn-off dependent diffusion/reaction parameters by the chemical reaction.

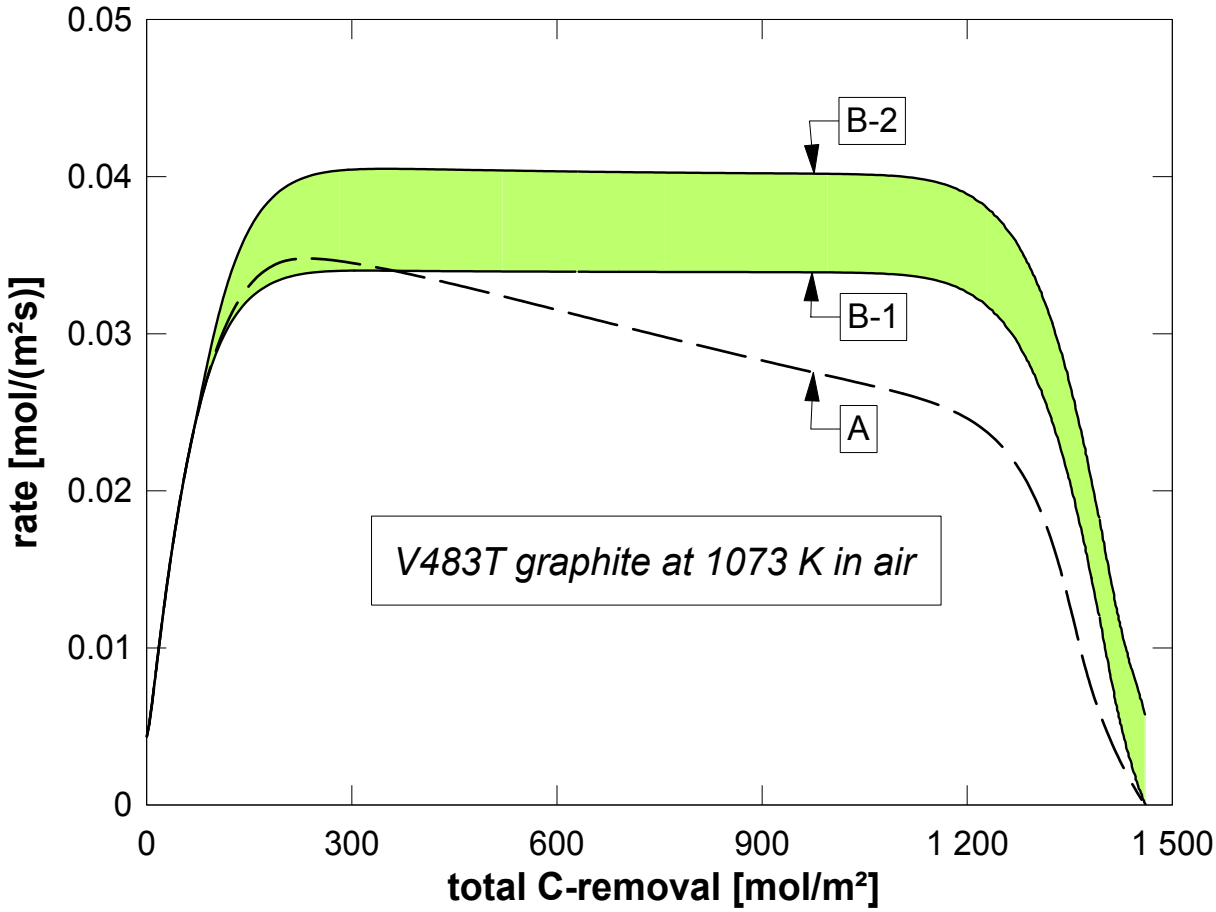

Fig.3-3: Calculated regime II rates vs. integral burn-off

Fig. 3-3 contains numerical solutions of eq. (2) for 1073 *K*: r_{II} vs. burn-off is given for different assumptions. Curve A represents a solution without consideration of any other weight loss than by chemical reaction. There is a strong rate increase, followed by slower decrease, which accelerates in the final stage. As explained before, such a behaviour is not observed under fast flow conditions, but may be found during oxidation in a thermogravimetric apparatus with small flow rates (low T). The rate increase is due to increase of reactivity and porosity with burn-off at low burn-off values. The rate decrease is caused by the dominating decrease of reactivity at high burn-off, which also leads to an effect similar to a diffusion boundary layer: In the outer regions with high burn-off, the diffusivity is high and the reactivity is small, and, accordingly, the mass transport resembles that in a boundary layer. Oxidation experience in regime II with flow however shows, that there is a continuous size reduction due to erosion by flow induced shear forces and some dust is usually found in these experiments (up to 20 % of the total weight loss for turbulent flow in tubes, *Re* = 2500). Rate curves B model oxidation rates considering erosion, which is roughly approximated by an erosion rate r_e depending on the outer burn-off by $r_e = 1.4 \cdot 10^{-6} \cdot (B_{x=0} - 0.4)^2$ *m/s* ($B_{x=0} \geq 0.4$). Erosion acts only on the outer surface. Curve B-1 contains the

chemical oxidation rate and curve B-2 the total C-removal rate (chemical reaction plus erosion). Both curves lead to a plateau value, as observed in regime II under flow; a rate decrease as in curve A does not occur, because the aforementioned boundary layer like effect does not exist and an equilibrium between erosion, renewing of the outer surface, and chemical reactions with diffusion is established. This results in oxygen concentration profiles, which move with nearly unchanged shape through the porous carbon, as the density (oxidation) profiles do; such oxygen concentration profiles are shown in Fig. 3-4 for different time steps.

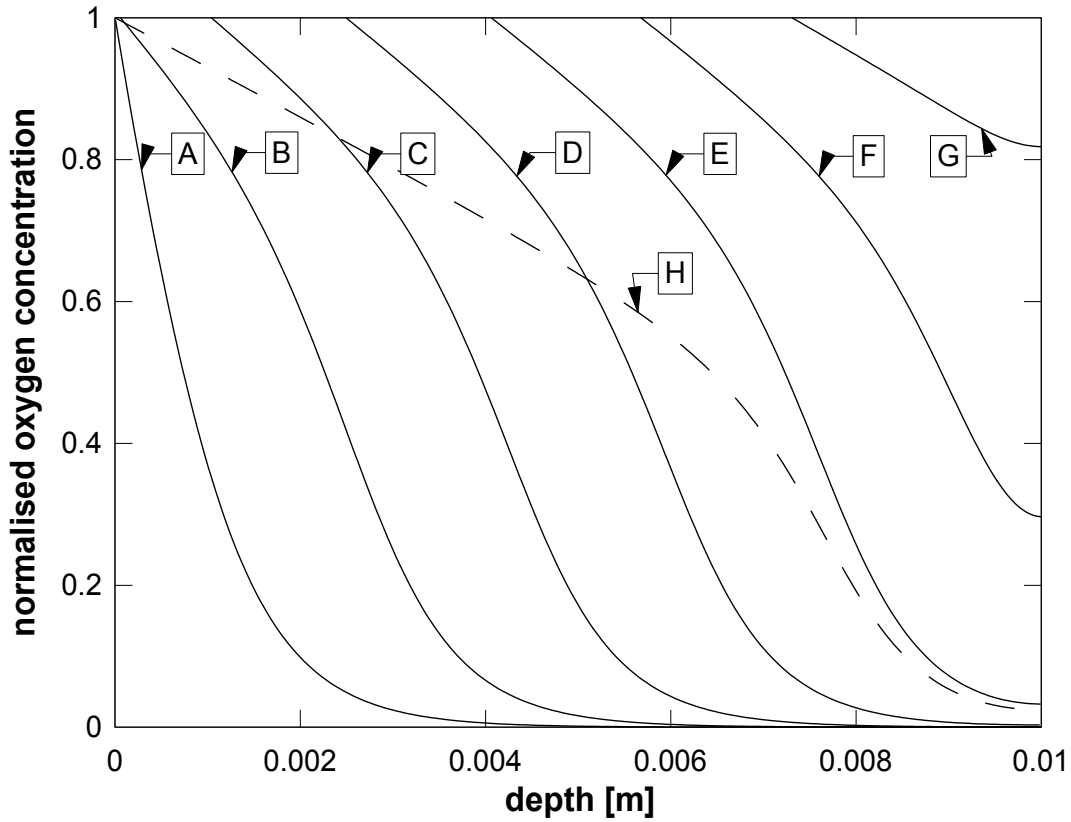

Fig. 3-4: Oxygen profiles in V483T at 1073 *K* in air (A: *t*=2000 *s*, Δ *t* of subsequent curves A-G: 4000 *s*; H: *t*= 30000 *s*)

For comparison one profile without calculation of erosion (H) is shown, too; the latter reveals the boundary layer like effect between 0 - 0.006 *m*. Depth of penetration of the oxidation effect is higher than estimated by usual formula, based on *B=0*, even if erosion is considered. Additional calculations were performed for transient rate behaviour in regime II: The answer of r_{II} on jumps in temperature is demonstrated in fig. 3-5 (V483T in air, starting temperature 1073 *K*, lower curve chemical reaction only, upper curve includes erosion). Rate r_{II} follows that jump, but because the aforementioned equilibrum is disturbed by temperature change, for a significant period of time resp. C-removal rate r_{II} changes its value until the equilibrium

oxidation profile for the actual temperature is reached. This transient behaviour has to be considered in evaluation of experimental r_{II}-data.

Comparison of these calculations with experiments in regime II, described resp. cited in a former paper [6], reveal sufficient agreement: Depth of penetration (density profiles) measured and calculated (considering different gas composition) are of the same size; for the increase of r_{II} with B a factor of 6 $\pm$ 3 was measured (this uncertainty is caused by the uncertainty of the measured starting value).

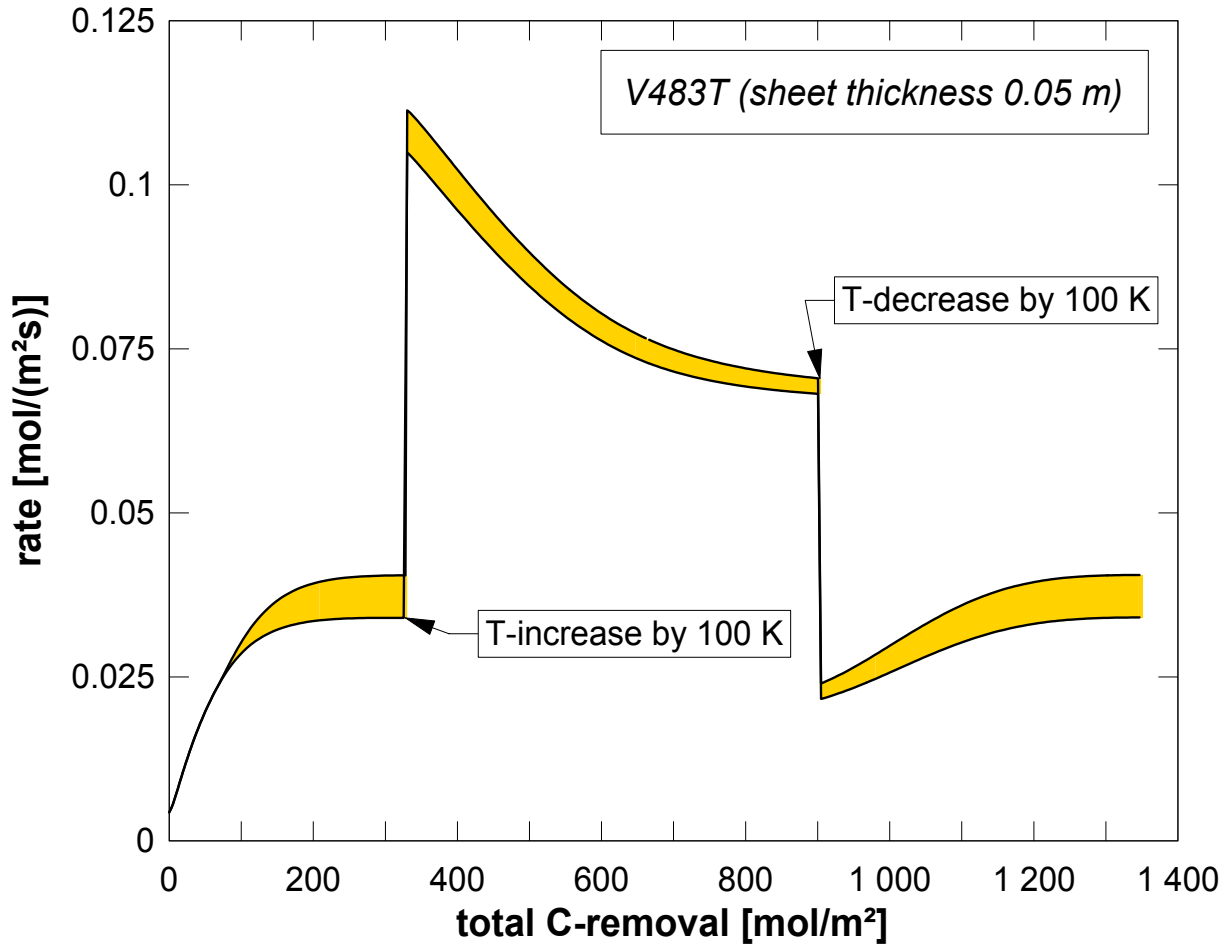

Fig. 3-5: Regime II rates during fast temperature changes

Considering, that ψ for low B used in calculations is probably to low due to neglection of dead end pores, the calculated increase factor of 9 might be overestimated; that can explain the disagreement. The burn-off resp. time range required to reach a stationary rate is in calculations larger than measured by up to a factor of 2; this might be due to uncertainties in the erosion function used. Agreement between measured and calculated stationary r_{II}-values

is still sufficient but suffers to some extent from the aforementioned differences between theoretical and measured apparent activation energies in regime II.

References

[1] H.-K. Hinssen, W. Katscher, R. Moormann: Jül-1875 (1983).

[2] H.-K. Hinssen, W. Katscher, R. Moormann: Jül-2052 (1986).

[3] H.-K. Hinssen, R. Moormann: Jül-2284 (1989).

[4] R. Moormann, S. Alberici, H.-K. Hinssen, C. H. Wu: Proc. 9th CIMTEC, Florence, Italy (1998).

[5] R. Moormann, H.-K. Hinssen, Ch Latge; J Dumesnil, A.C. Veltkamp, V. Grabon, D. Beech, D. Buckthorpe, T. Dominguez, A-K. Krüssenberg, C.H. Wu: Nuclear science, OECD Procedings, Paris, France (1999) 161 – 172.

[6] R. Moormann, S. Alberici, H.-K. Hinssen, A.-K. Krüssenberg, C. H. Wu: Adv. Sci Tech 24 (1999) 331 – 8.

[7] P.L. Walker, F. Rusiko, G. Austin: Adv. Catalysis XI (1995) 133 – 221.

[8] H.-K. Hinssen, A.-K. Krüssenberg, R. Moormann, C.H. Wu: Proc. 10th IUPAC-Conf. On High Temperature Materials Chemistry, Jülich, 10.-14.04.2000.

[9] R. Aris: The mathematical theory of diffusion and reaction in permeable catalysts. Oxford (1975).

[10] H.-K. Hinssen, R. Moormann, W. Katscher: Proc. Jahrestagung Kerntechnik'86 (1986), Aachen 211-4 (ISSN 0720-9207).

[11] J. D. Clark, C.S. Gghanthan, P. J. Robinson: J. Mater. Sci. 14 (1979) 2937.

[12] J. E. Crank: The Mathematics of Diffusion. 2nd ed. Oxford (1975), Chapter 14.2.

Annex: final report:

Chemical kinetic data for advanced oxidation models

I Parameters derived for the advanced oxidation models

The kinetic data in advanced oxidation models are strictly associated with the application of reaction dependent parameters, which were used in oxidation equations of these models. These parameters are

- activation energy (E_A)
- Burn off dependence of the reaction rate
- pre-exponential factor (k)
- concentration of the reaction gas (c)

The activation energy is given by :

$$-E_A = R\frac{d\ln RG}{d1/T}$$

The pre-exponential factor is to be calculated by:

$$k = \frac{RG}{e^{-\frac{E_A}{RT}} * c/c_0}$$

E_A = activation energy; RG = reaction rate; R = gas constant; T = temperature; c= concentration of the reaction gas

I.I Oxidation in steam

The burn off dependent reaction rates adapted from the measured values are given in Tab.1:

Tab.1: Burn off dependent reaction rates for oxidation in steam at 1173 and 1253 K in [%/s]

Graphite:	**A3-3**		**V483T5**	
Temperature	**1173 K**	**1253 K**	**1173 K**	**1253 K**
Binder Maximum*	1,10E-03	3,92E-03	-	-
10% Burn off	7,15E-04	2,78E-03	5,18E-04	1,50E-03
20% Burn off	6,56E-04	1,71E-03	5,61E-04	2,30E-03
30% Burn off	6,30E-04	1,50E-03	5,98E-04	2,25E-03
40% Burn off	6,40E-04	1,19E-03	6,01E-04	2,00E-03
50% Burn off	6,91E-04	8,70E-04	5,96E-04	1,74E-03

* = 5%

On the basis of the reaction rates, the activation energies were calculated exemplary for binder maximum, 25 % burn off and peak maximum (Tab.2).

Tab. 2: Calculated activation energies for according burn off values

Graphite	**E_A : A3-3**	**E_A : V483T5**
Binder Maximum	194 [kJ/mol]	-
25 % Burn off	139 [kJ/mol]	-
Peak maximum	-*	196 [kJ/mol]

* = no second peak maximum has been observed at oxidation at 1173 K

I.II Oxidation in air

The examination of the advanced oxidation parameters of the fuel element matrix graphite A3-27 are already given in fig. 2-5 of the report. The calculation of separated binder and filler peaks and the resulting activation energies are shown in this figure. The data of the graphite V483T is already published and reported in reference [8].

Comprising, the activation energies of these graphites are give in Tab. 3:

Tab. 3: activation energies for oxidation in air

Graphite	**E_A : A3-27**	**E_A : V483T5**
Binder maximum	123 [kJ/mol]	-
Filler maximum	166 [kJ/mol]	-
Peak maximum	-	166 [kJ/mol]